Optimized Dispersion Compensation Using Orthogonal Frequency-Division Multiplexing

Daniel J. F. Barros and Joseph M. Kahn, *Fellow, IEEE*

Abstract—**Orthogonal frequency-division multiplexing (OFDM) can compensate for linear distortions, such as group-velocity dispersion (GVD) and polarization-mode dispersion (PMD), provided the cyclic prefix is sufficiently long. Typically, GVD is dominant, as it requires a longer cyclic prefix. Assuming coherent detection, we show how to analytically compute the minimum number of subcarriers and cyclic prefix length required to achieve a specified power penalty, trading off power penalties from the cyclic prefix and from residual inter-symbol interference (ISI) and inter-carrier interference (ICI). We derive an analytical expression for the power penalty from residual ISI and ICI.**

Index Terms—**Coherent optical communications, communications system performance, group-velocity dispersion, multi-carrier optical systems, orthogonal frequency-division multiplexing, polarization-mode dispersion.**

I. INTRODUCTION

ORTHOGONAL frequency-division multiplexing (OFDM) is a multi-carrier modulation that has been extensively investigated and deployed in wireless and wireline communications [1], [2]. It is receiving increased interest in the fiber-optic research community for its robustness against inter-symbol interference (ISI), since the symbol period of each subcarrier can be made long compared to the delay spread caused by group-velocity dispersion (GVD) and polarization-mode dispersion (PMD) [3], [4]. Although single-carrier and multi-carrier systems using coherent detection have fundamentally the same power and spectral efficiencies for a given modulation format in the presence of unitary impairments such as GVD and PMD, there may be differences due to practical constraints.

Experiments have been performed demonstrating the potential of OFDM with coherent detection in optical systems [4], [5], but very little closed-form performance analysis has been performed to date. In principle, the impulse response due to GVD has infinite duration, so the proper choice of cyclic prefix length is not obvious. If the cyclic prefix is too short relative to the impulse response duration, ISI and inter-carrier interference (ICI) will occur. On the other hand, if the cyclic prefix is excessively long relative to the number of subcarriers, the sampling rate

must be increased significantly, and a large fraction of the transmitted energy is wasted in cyclic prefix samples, leading to a substantial power penalty. For a given cyclic prefix length, these penalties can be reduced to an arbitrary degree by increasing the number of subcarriers.

In practice, however, it may be desirable to minimize the number of subcarriers employed. For example, it is known that the peak-to-average power ratio is proportional to N_c, the number of subcarriers [1]. OFDM signals are modulated using Mach–Zehnder (MZ) modulators having nonlinear, peak-limited transfer characteristics [6], [7], so minimizing N_c will help maximize optical power efficiency in the modulator. As another example, laser phase noise destroys the orthogonality between subcarriers, causing ICI. It has been shown that for a given laser linewidth, the variance of ICI is proportional to N_c [8], so minimizing N_c can help in combating laser phase noise. Hence, in this paper, assuming coherent detection, we find the minimum number of subcarriers and cyclic prefix length that achieve low power and sampling penalties in the presence of GVD and PMD.

This paper is organized as follows. In Section II, we review the fundamentals of multi-carrier systems. We introduce the canonical OFDM model and determine the minimum oversampling ratio required to avoid aliasing. In Section III, we focus on GVD, and derive analytical expressions for the ISI and ICI incurred when an insufficient cyclic prefix is used. We use these expressions to compute power penalties for representative examples, comparing the results to simulations. We compare the performance of OFDM to single-carrier systems. In Section IV, we consider first-order PMD, and discuss how to extend the analysis to arbitrary-order PMD. We consider both single- and dual-polarization receivers.

II. OFDM THEORY

A. OFDM Review

In OFDM, the inverse discrete Fourier transform (IDFT) and DFT are used to modulate and demodulate the data constellations on the subcarriers, as shown in Fig. 1. The IDFT and DFT replace the banks of analog I/Q modulators and demodulators that would otherwise be required. To show the equivalence between OFDM and analog multi-carrier systems, we can write the OFDM signal as

$$x_{ofdm}(t) = \sum_k \sum_{q=0}^{N_c-1} X_{q,k} b(t - kT_{\text{sym}}) e^{j2\pi q f_d t} \quad (1)$$

where $X_{q,k}$ denotes the qth subcarrier constellation symbol transmitted on the kth OFDM symbol, $b(t)$ is a pulse shape,
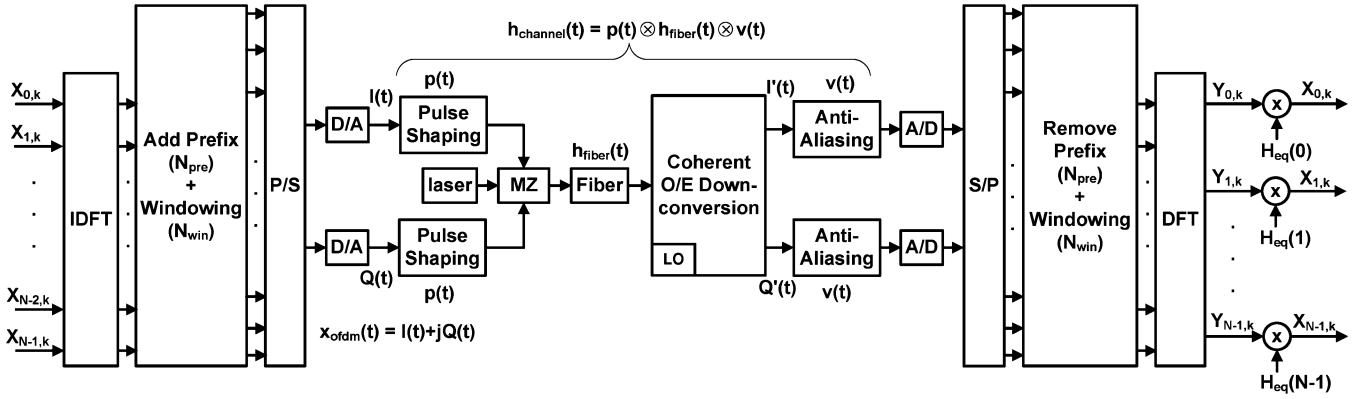
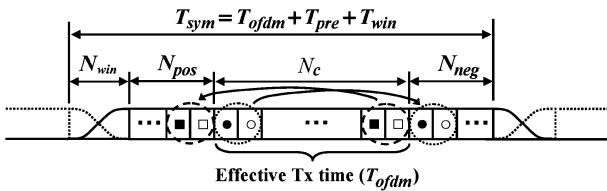Fig. 1.   Digital implementation of OFDM transmitter and receiver.

Fig. 2.   OFDM symbol, including the cyclic prefix and windowing.

$T_{\text{sym}} = (N_c + N_{\text{pre}} + N_{\text{win}})T_c = T_{ofdm} + T_{pre} + T_{win}$ is the OFDM symbol period and $f_d = 1/(N_c T_c)$ is the frequency separation between subcarriers. We define T_c as the sample or chip period, and N_c, N_{pre} and N_{win} are integers. If (1) is sampled every chip period, we have

$$x_{ofdm}(nT_c) = \sum_k \sum_{q=0}^{N_c-1} X_{q,k} b(nT_c - kT_{\text{sym}}) e^{j\frac{2\pi qn}{N_c}}. \quad (2)$$

An OFDM symbol corresponds to $N_c + N_{\text{pre}} + N_{\text{win}}$ samples or chips, as shown in Fig. 2. The block of N_c samples in (2) corresponds to the IDFT. The remaining N_{pre} and N_{win} terms are a periodic extension of the OFDM signal known as the *cyclic prefix*, and pulse shaping known as *windowing*. The cyclic prefix is used so that the sequence of received chips in one symbol is equivalent to one period of a circular convolution between the transmitted OFDM symbol $x_{ofdm}(t)$ and the chip-rate samples of the channel impulse response $h_{\text{channel}}(t)$. In the frequency domain, this corresponds to the multiplication of subcarrier q by the corresponding sample of the channel frequency response $H_{\text{channel}}(\omega)$. Thus, a single-tap equalizer on subcarrier q can be used to invert any amplitude and phase distortion introduced by the channel, i.e., $H_{eq}(q) = H_{\text{channel}}^{-1}(2\pi f_s q/N_c)$. For our system, the channel frequency response $H_{\text{channel}}(\omega)$ is given by

$$H_{\text{channel}}(\omega) = P(\omega)H_{\text{fiber}}(\omega)V(\omega) \quad (3)$$

where $P(\omega)$ and $V(\omega)$ are the pulse-shaping and anti-aliasing filters and $H_{\text{fiber}}(\omega)$ represents the fiber frequency response. The cyclic prefix samples ($N_{\text{pre}} = N_{\text{pos}} + N_{\text{neg}}$) are appended to the signal after the IDFT. Ideally, the cyclic prefix length should be no smaller than the duration of the channel impulse response $h_{\text{channel}}(t)$.
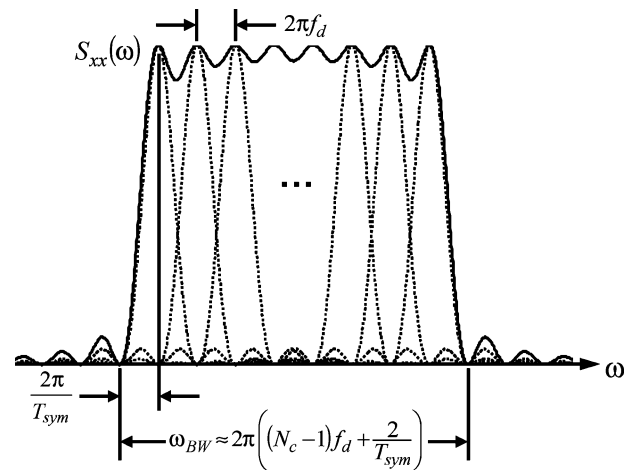

Fig. 3.   OFDM spectrum, assuming rectangular windowing ($N_{\text{win}} = 0$).

The additional N_{win} samples are used to control the OFDM spectrum by introducing additional pulse shaping. Common choices for the window functions include rectangular and raised-cosine pulses [1], [2]. The rectangular window corresponds to $N_{\text{win}} = 0$. Assuming a rectangular window and uncorrelated transmitted symbols, $E[x_{n,k}x_{l,m}^*] = 0$ for $n \neq l$, the power spectrum of $x_{ofdm}(t)$ is given by

$$S_{xx}(\omega) = \frac{T_{\text{sym}}}{N_c^2} \sum_{q=0}^{N_c-1} P_q \text{sinc}^2 \left(\frac{T_{\text{sym}}}{2\pi}(\omega - 2\pi q f_d) \right) \quad (4)$$

where $P_q = E[|X_q|^2]$ is the average power per symbol on subcarrier q. A plot of (4) is shown in Fig. 3, assuming all subchannels have equal powers.

We note in Fig. 3 that the OFDM spectrum resembles an ideal rectangular shape and has a bandwidth approximately given by

$$\omega_{BW} \approx 2\pi \left((N_c - 1)f_d + \frac{2}{T_{\text{sym}}} \right) \leq 2\pi(N_c + 1)f_d. \quad (5)$$

To achieve a desired symbol rate R, the frequency separation between subcarriers ($f_d = 1/N_c T_c$) must be equal to $f_d = (N_c + N_{\text{pre}})/N_c \times R/N_c$. Thus, (5) can be rewritten as

$$\omega_{BW} \approx 2\pi \frac{(N_c + 1)}{N_c} \frac{(N_c + N_{\text{pre}})}{N_c} R. \quad (6)$$

In the case of the rectangular window, the OFDM spectrum has significant sidelobes, as shown in Fig. 3. These can be reduced by using alternate windows, such as the raised-cosine, which require $N_{\text{win}} > 0$. Alternately, the sidelobes can be reduced by using a pulse-shaping filter $p(t)$ after the digital-to-analog converter (D/A).

The symbols extensions required for the cyclic prefix (N_{pre}) and windowing (N_{win}) represent penalties, since they do not carry useful information and are discarded at the receiver. They represent a *power penalty* because a portion of the energy is wasted on these samples and also a *sampling penalty* because the chip rate $1/T_c$, which is equal to the sampling frequency, has to be higher to maintain the desired symbol rate R, i.e., $f_s = 1/T_c = (N_c + N_{\text{pre}} + N_{\text{win}})/N_c \times R$.

For typical values used in OFDM systems, the OFDM bandwidth given by (6) is very close to the Nyquist bandwidth, i.e., $\omega_{BW} \approx \omega_{Ny} = 2\pi \times R$. The confined spectrum of OFDM is a practical advantage over single-carrier systems where, the 90% power bandwidth is typically of order $\omega_{sc} \approx 2\pi \times 2R$ [9]. Another important advantage of OFDM is in the minimum required oversampling ratio. In OFDM, oversampling is performed by not modulating the edge subcarriers in Fig. 1, i.e., by inserting zero subcarriers. Assuming that only N_u of the N_c subcarriers are modulated, the oversampling ratio is $M_s = N_c/N_u$. In OFDM, it is possible to employ arbitrary rational oversampling ratios, unlike single-carrier transmission, where this may require complex signal processing. Since the OFDM spectrum falls off more rapidly than a single-carrier spectrum, lower oversampling ratios can be employed. We have found that when the pulse-shaping and anti-aliasing filters are chosen properly, an oversampling ratio $M_s = 1.2$ is sufficient to avoid aliasing, while single-carrier systems typically require an oversampling ratio $M_s = 1.5$ or 2 [10]. Finally, we note that the expressions defined previously are also valid when oversampling is used, provided that N_{pre} and N_{win} are scaled to reflect the oversampling ratio, i.e., $N_{\text{pre}}(M_s) = M_s \times N_{\text{pre}}(M_s = 1)$ and $N_{\text{win}}(M_s) = M_s \times N_{\text{win}}(M_s = 1)$ and the sampling frequency is scaled by the oversampling ratio, i.e., $f_s = 1/T_c = M_s \times R \times (N_c + N_{\text{pre}}(M_s) + N_{\text{win}}(M_s))/N_c$.

III. GROUP-VELOCITY DISPERSION

A. Theory

Fiber GVD spreads the transmitted symbols, causing ISI that degrades the error probability. The fiber frequency response in the presence of GVD is given by

$$H_{\text{fiber}}(\omega) = e^{-j\omega^2 \frac{\beta_2}{2} L} \tag{7}$$

where β_2 is the fiber GVD parameter and L is the fiber length. Although the receiver employs a single-tap equalizer on each subcarrier to invert the channel, ISI can occur when the cyclic prefix is insufficient, so that symbols in a neighboring block overlap with the symbol of interest. In order to avoid ISI, ideally, the cyclic prefix duration T_{pre} should no smaller than the duration of the impulse response $h_{\text{channel}}(t)$. However, GVD leads to an infinite-duration impulse response, and the tails of the im-
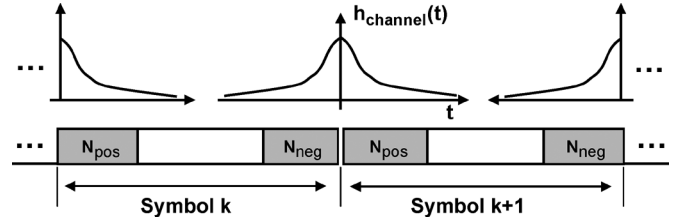

Fig. 4. OFDM symbol with insufficient cyclic prefix.

pulse response not covered by the cyclic prefix lead to residual ISI, as shown in Fig. 4.

Referring to Fig. 4, note that ISI on symbol k comes both from symbols $k-1$ and $k+1$, since the channel impulse response is two-sided. If $N_{\text{pre}} = N_{\text{pos}} + N_{\text{neg}}$ samples are used for the cyclic prefix and if the channel impulse response has positive and negative lengths $L_p - 1$ and $L_n - 1$, respectively, the residual ISI on the nth time-domain sample in the kth OFDM symbol interval can be written as

$$\text{ISI}_k(n) = \sum_{r=N_{\text{pos}}+1}^{L_p-1} x_{k-1}(n + N_c + N_{\text{pre}} + N_{\text{pos}} - r)h_{\text{channel}}(r)$$
$$+ \sum_{u=-L_n+1}^{-N_{\text{neg}}-1} x_{k+1}(n - N_c - N_{\text{neg}} - u)h_{\text{channel}}(u). \tag{8}$$

In Appendix A, we show that if the transmitted symbols are uncorrelated and if $N_c > \max(L_p - N_{\text{pos}} - 1, L_n - N_{\text{neg}} - 1)$, after the DFT, the ISI variance on subcarrier q is given by

$$\sigma_{\text{ISI}}^2(q) = \sigma_s^2 \left(\sum_{p=N_{\text{pos}}+1}^{L_p-1} |H_p(q)|^2 + \sum_{n=-L_n+1}^{-N_{\text{neg}}-1} |H_n(q)|^2 \right) \tag{9}$$

where $\sigma_s^2 = E[|x(n)|^2]$ is the mean power per sample in the time-domain waveform, and $H_p(q)$ and $H_n(q)$ are the N_c-point DFTs of the positive and negative tails of the channel impulse response, respectively. They can be written as

$$H_p(q) = \sum_{v=p}^{L_p-1} h_{\text{channel}}(v)e^{-j2\pi vq/N_c}$$
$$H_n(q) = \sum_{v=N_c-L_n}^{N_c-1-n} h_{\text{channel}}(v)e^{-j2\pi vq/N_c}. \tag{10}$$

Moreover, since the linear convolution with the channel can no longer be considered as one period of a circular convolution, inter-carrier interference (ICI) will occur within the kth symbol. In Appendix A, we show that the ICI has the same variance as the ISI. Thus, the variance of the total interference on subcarrier q is given by

$$\sigma_{\text{ISI+ICI}}^2(q) =$$
$$2\sigma_s^2 \left(\sum_{p=N_{\text{pos}}+1}^{L_p-1} |H_p(q)|^2 + \sum_{n=-L_n+1}^{-N_{\text{neg}}-1} |H_n(q)|^2 \right). \tag{11}$$

In order to compute the probability of symbol error, we must also take into account the power penalty of the cyclic prefix.
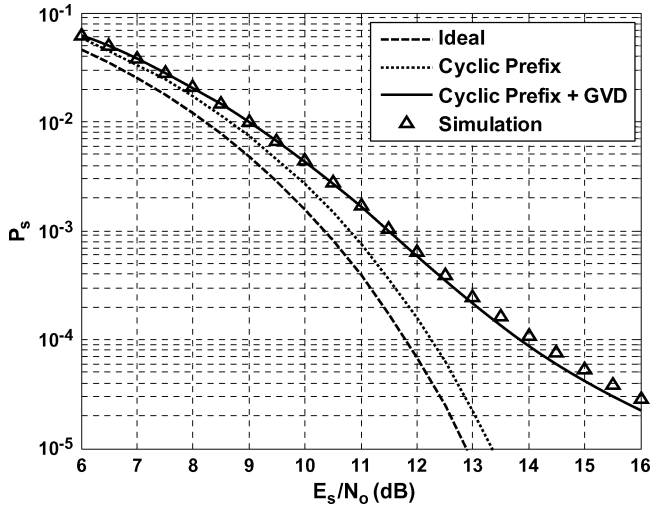
Fig. 5. Probability of symbol error in presence of GVD for $L = 80$ km, $D = 17$ ps/(nm.km), $N_c = 64$, $N_u = 52$, $N_{\text{pre}} = 5$ and $R = 26.7$ GHz.
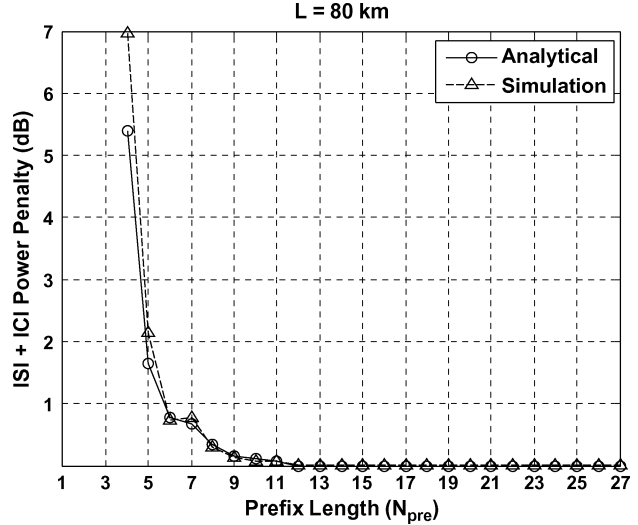

Fig. 6. ISI+ICI power penalty at $P_S = 10^{-4}$ for $L = 80$ km, $D = 17$ ps/(nm.km), $N_c = 64$, $N_u = 52$ and $R = 26.7$ GHz.
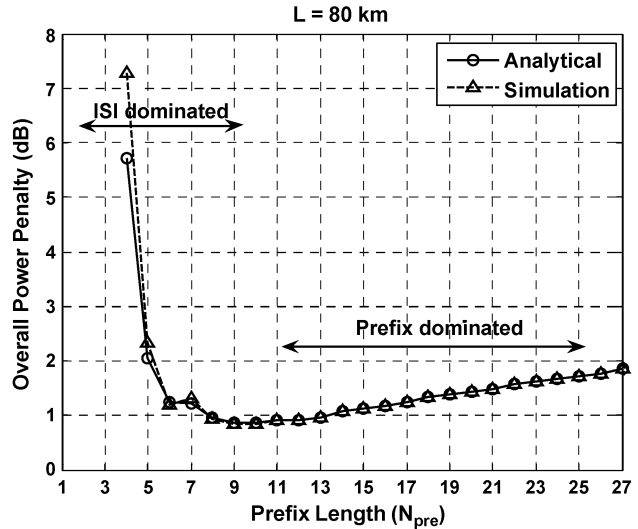

Fig. 7. Overall power penalty at $P_S = 10^{-4}$ for $L = 80$ km, $D = 17$ ps/(nm.km), $N_c = 64$, $N_u = 52$ and $R = 26.7$ GHz.

If we assume that only N_u of the N_c subcarriers are used, the probability of symbol error for 4-QAM-modulated subcarriers can be written as

$$P_s = \frac{1}{N_u}$$
$$\times \sum_{q=0}^{N_u-1} erfc \left(\sqrt{\frac{1}{2} \left(\frac{N_u}{N_{\text{pre}} + N_u} \right) \left(\frac{P_q}{\sigma_0^2 + \sigma_{\text{ISI+ICI}}^2(q)} \right)} \right) \quad (12)$$

where $N_u/(N_u + N_{\text{pre}})$ is the extra energy wasted on the cyclic prefix samples, P_q is the average power per symbol of subcarrier q, σ_0^2 is the variance of sampled additive white Gaussian noise ($\sigma_0^2 = N_0 R$), and $\sigma_{\text{ISI+ICI}}^2(q)$ is the variance of the total interference on subcarrier q.

B. Simulation Results

We assume that fiber nonlinearity and laser phase noise effects are either negligible or have been compensated, so the fiber may be modeled as a linear channel. Therefore, the only impairments in the system are GVD and PMD. In order to minimize the sampling penalty, at the transmitter, we use a rectangular window, and perform pulse shaping using a fifth-order Butterworth lowpass filter having a 3-dB cutoff frequency equal to half the bandwidth of the OFDM signal, given by (6). At the receiver, the anti-aliasing filter is an identical Butterworth lowpass filter. We assume transmission of 53.4 Gb/s in one polarization. The subcarriers are modulated using 4-QAM and a FEC code with an overhead of 255/239, so the symbol rate is $R = 26.7$ GHz.

As an initial example, we consider a fiber length of 80 km with a dispersion $D = 17$ ps/(nm·km). The FFT size is 64 and the oversampling ratio is $M_s = 1.2$, i.e. only 52 subcarriers are used. The minimum required oversampling ratio of $M_s = 1.2$ was determined by adding zero subcarriers until noise aliasing became negligible [1]. The cyclic prefix length, referred to an oversampling ratio $M_s = 1$, is 5 samples. A plot of the symbol-error probability for this example is shown in Fig. 5.

In Fig. 5, it can be observed that the power penalty increases at small P_s. Since the majority of the FEC codes have a threshold

around $P_s = 10^{-3}$, we will measure the power penalty at $P_s = 10^{-4}$ in order to have some margin.

Figs. 6 and 7 illustrate the ISI+ICI penalty and the overall penalty, respectively, as a function of the cyclic prefix length, holding the data rate constant.

In Fig. 7, we observe that the overall power penalty has two different regions: ISI+ICI-dominated and cyclic prefix-dominated. In the former, the cyclic prefix is much shorter than the fiber impulse response and therefore severe ISI+ICI occur, impairing the system performance. In the latter region, the cyclic prefix is sufficiently long that the ISI+ICI are negligible, but a large fraction of the transmitted energy is wasted on the cyclic prefix samples, leading to a power penalty. For example, for the same scenario as in Fig. 7, if one chose a cyclic prefix length such that 98% or 95% of the fiber's impulse response energy was contained in that same duration, one would be required to use a cyclic prefix length of 14 and 12 samples, respectively, while the optimum cyclic prefix is 9 samples. The optimum
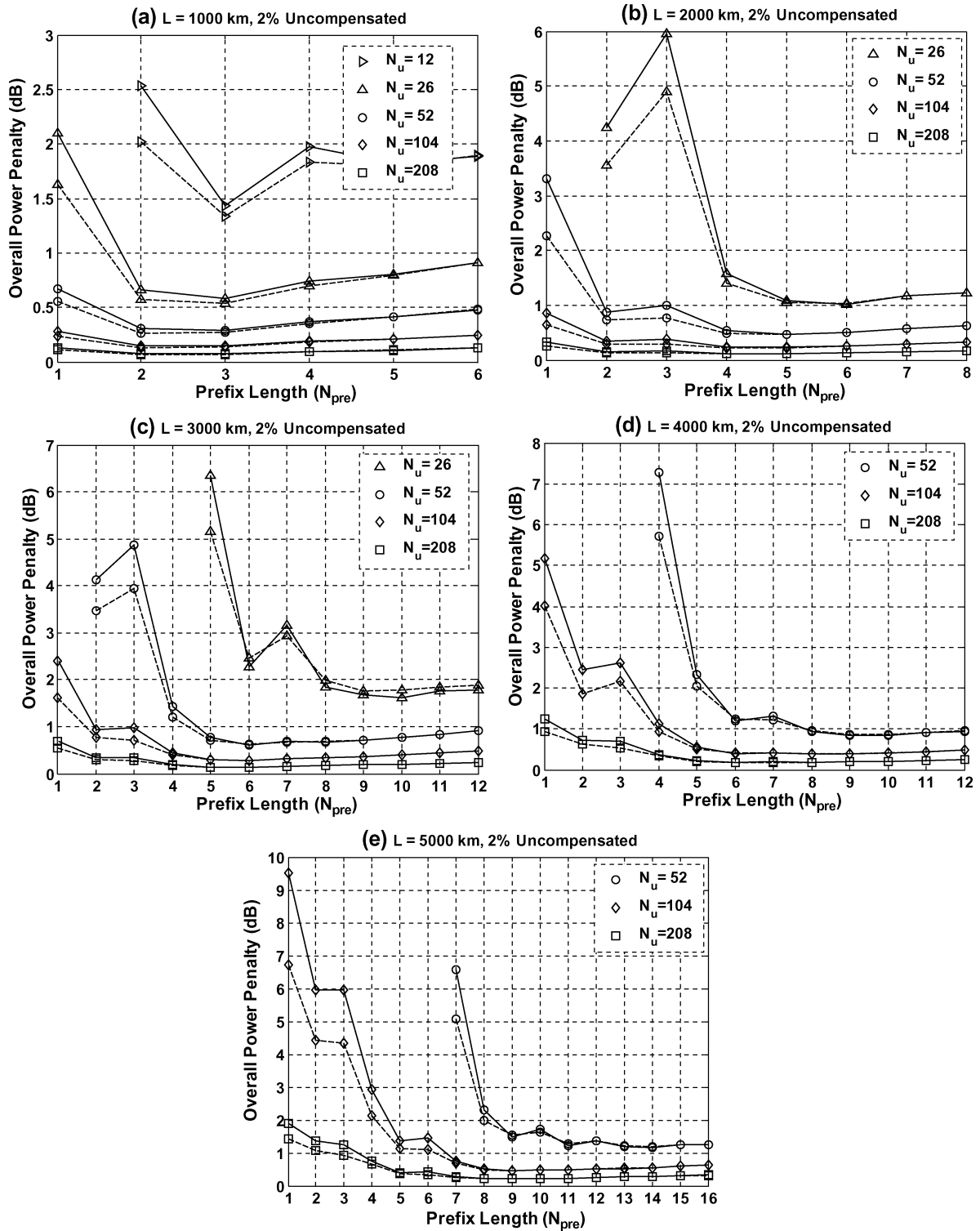
Fig. 8. Overall power penalties at $R = 26.7$ GHz for 2% undercompensated GVD lengths of (a) 1000 km, (b) 2000 km, (c) 3000 km, (d) 4000 km, and (e) 5000 km. The dashed lines $(--)$ are the analytical values and the solid lines $(—)$ are the simulation results.

cyclic prefix length results in a penalty from ISI+ICI equal to the penalty from energy wasted in the cyclic prefix samples.

As explained above, it may be desirable to minimize the number of subcarriers employed. Hence, we would like to calculate the minimum combination of number of subcarriers and cyclic prefix that generate a specified power penalty. For concreteness, we consider a system transmitting at a symbol

rate $R = 26.7$ GHz through fiber spans having dispersion $D = 17$ ps/(nm · km), with 98% inline optical dispersion compensation (i.e., the residual dispersion is 0.34 ps/(nm · km)). Fig. 8 shows the overall power penalties for fiber lengths between 1000 km and 5000 km.

In Figs. 6, 7, and 8, we observe some discrepancies between the simulation and theoretical results. Equations (11) and (12)

TABLE I
OFDM PARAMETERS FOR 53.4 Gb/s

Total Length (km)	Residual Dispersion D·L.(ps/nm)	DFT Size N_c	Modulated Subcarriers N_u	Cyclic Prefix N_{pre}
1000	340	32	26	3
2000	680	64	52	4
3000	1020	64	52	6
4000	1360	128	104	6
5000	1700	128	104	8

Number of subcarriers and cyclic prefix required to achieve an overall power penalty less than 1 dB. We consider 4-QAM subcarriers, $R = 26.7$ GHz, $D = 17$ ps/$(\mathrm{nm} \cdot \mathrm{km})$ with 98% inline optical dispersion compensation.
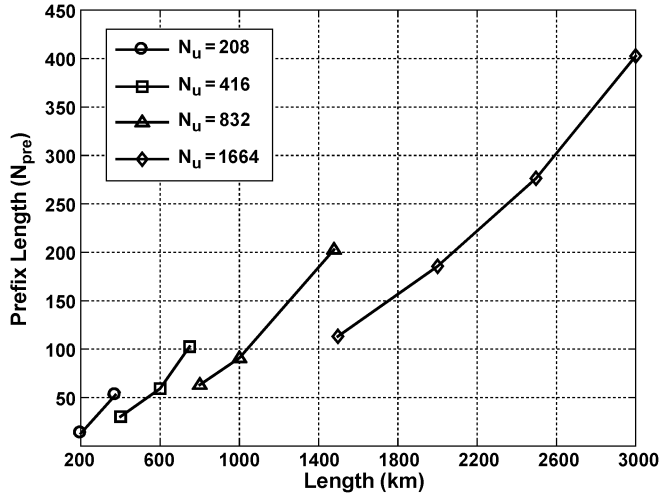

Fig. 9. Optimum number of used subcarriers and cyclic prefix length as a function of the fiber length for $R = 26.7$ GHz when no optical dispersion compensation is used.

are exact given that there is no correlation between the OFDM chips. This condition is satisfied only if the transmitted symbols are uncorrelated and if the oversampling ratio M_s is equal to 1, i.e., no oversampling. Since an oversampling ratio $M_s = 1.2$ is required to avoid aliasing (with the Butterworth filters we have used), (11) and (12) are only an approximation of the ICI+ICI variance, as explained in Appendix A. The error is maximum when the cyclic prefix length is short since it corresponds to the situation of highest ISI+ICI. However, we verified that for high ISI/ICI, (11) predicts the ISI+ICI variance with a maximum error on the order of 10%–15% when $M_s = 1.2$.

In Figs. 6, 7 and 8, we can also observe that in some cases increasing the cyclic prefix length also increases or maintains the power penalty. This is because increasing the cyclic prefix length while keeping the data rate constant requires increasing the chip rate which, in turn, increases the OFDM bandwidth, increasing the temporal spread caused by GVD. On the other hand, a longer cyclic prefix can compensate longer tails of the impulse response. It is not obvious which effect will dominate. When the additional pulse spreading is longer than the increased cyclic prefix length, the overall power penalty increases.

From Fig. 8, we can extract the minimum number of subcarriers and cyclic prefix required to achieve a desired power penalty. The values required to achieve a penalty of 1 dB are given in Table I.

Note that by making other choices of these parameters, it is possible to make the total penalty arbitrarily small. As the

uncompensated dispersion becomes larger, this may involve choosing a very large number of subcarriers, which may be undesirable, for reasons cited above. In choosing these parameters, one should note that some synchronization schemes used in practice require that the cyclic prefix length exceeds a certain fraction of the total number of subcarriers [11], [12]. The results presented in Table I are compatible with those synchronization schemes.

Finally, in Fig. 9 we plot the optimum number subcarriers and cyclic prefix length as a function of the fiber length when no optical dispersion compensation is used.

IV. POLARIZATION-MODE DISPERSION

A single-mode fiber with PMD can be described by a frequency-dependent Jones matrix [13]–[16]. Input and output signals can be described by two-component Jones vectors.[1] The input and output time-domain signals are denoted by $\mathbf{x(t)} = [x_1(t) \ x_2(t)]^{\mathrm{T}}$ and $\mathbf{y(t)} = [y_1(t) \ y_2(t)]^{\mathrm{T}}$, respectively. Their Fourier transforms can be related as

$$\begin{bmatrix} Y_1(\omega) \\ Y_2(\omega) \end{bmatrix} = \mathbf{R_2} \mathbf{\Lambda} \mathbf{R_1^{-1}} \begin{bmatrix} X_1(\omega) \\ X_2(\omega) \end{bmatrix}. \tag{13}$$

Assuming first-order PMD, $\mathbf{R_1}$ and $\mathbf{R_2}$ are frequency-independent rotation matrices representing a change of basis into the input and output principal states of polarization (PSPs), respectively, and $\mathbf{\Lambda}$ is a frequency-dependent matrix representing the delay between the fast and slow PSPs [13]–[15]. Explicit expressions for $\mathbf{R_i}$ and $\mathbf{\Lambda}$ [15], [16] are

$$\mathbf{R_i} = \begin{bmatrix} r_{1i} & -r_{2i}^* \\ r_{2i} & r_{1i}^* \end{bmatrix} \quad \mathbf{\Lambda} = \begin{bmatrix} e^{j\omega\tau/2} & 0 \\ 0 & e^{-j\omega\tau/2} \end{bmatrix} \tag{14}$$

where

$$r_{1i} = \cos\theta_i \cos\varepsilon_i - j\sin\theta_i \sin\varepsilon_i$$
$$r_{2i} = \sin\theta_i \cos\varepsilon_i + j\cos\theta_i \sin\varepsilon_i. \tag{15}$$

The θ_i, ε_i are independent random variables representing the fast PSP azimuth and ellipticity angles, respectively. τ is a random variable representing differential group delay (DGD) Considering GVD and first-order PMD, the fiber frequency response is then

$$\mathbf{H_{fiber}}(\omega) = \begin{bmatrix} H_2(\omega) \\ H_1(\omega) \end{bmatrix} = \mathbf{R_2} \mathbf{\Lambda} \mathbf{R_1^{-1}} e^{-j\omega^2 \frac{\beta_2}{2} L}. \tag{16}$$

We will now discuss two approaches to reception in the presence of PMD. The first approach uses a dual-polarization receiver and the second approach uses a single-polarization receiver with polarization control.

A. Dual-Polarization Receiver

A dual-polarization receiver enables electronic polarization control and the use of polarization-multiplexed signals which can double the bit rate. An OFDM polarization-multiplexed system is shown in Fig. 10.

The transmitter consists of two independent OFDM modulators. The two modulated optical signals are combined in orthogonal polarizations using a polarization beam splitter (PBS).

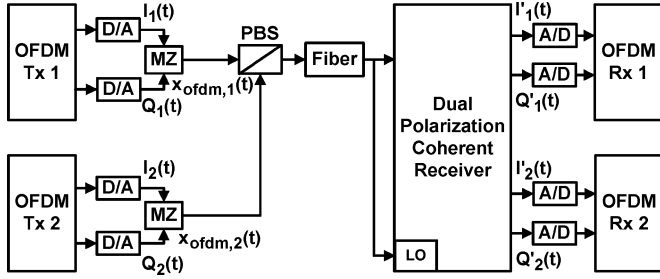[1]We use boldface variables to denote vectors and matrices.

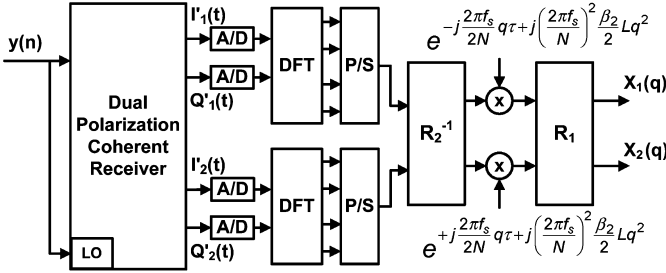Fig. 10. OFDM polarization-multiplexed system.

Fig. 11. Combined PMD and GVD equalizer for an OFDM polarization-multiplexed system.

After passing through single-mode fiber, the received signal is split into two copies, which are mixed with the LO in two orthogonal polarizations. Each polarization is detected using a $90°$ hybrid and two balanced photodetectors. The electrical outputs are the in-phase and quadrature components associated with the two orthogonal polarizations. These signals are then low-pass filtered and sampled [10].

The dual-polarization receiver can also be used with a single-polarization transmitter. In this case, one of the transmitters of Fig. 10 would not be used.

In order to compensate for PMD and GVD, the receiver must invert the fiber frequency response. The equalizer corresponds then to a 2×2 matrix multiplication between the signals in the two polarizations on each subcarrier q after the DFT operation. For first-order PMD, it can be written as

$$\mathbf{H_{eq}(q)} = \mathbf{H_{fiber}^{-1}}\left(\frac{2\pi \mathbf{f_s q}}{\mathbf{N_c}}\right) = \mathbf{R_1}\mathbf{\Lambda^{-1}}\mathbf{R_2^{-1}}e^{+j\left(\frac{2\pi f_s}{N_c}\right)^2\frac{\beta_2}{2}Lq^2}. \tag{17}$$

In writing down (17), for simplicity, we have not included the pulse-shaping and anti-aliasing filters. Fig. 11 shows the combined equalizer for PMD and GVD.

In the absence of polarization-dependent losses, using a dual-polarization receiver, PMD causes no loss of information, since PMD is a unitary transformation. In order to avoid ISI, the cyclic prefix length should be no smaller than the duration of the channel impulse response. For example, to compensate

first-order PMD only (in the absence of GVD), the cyclic prefix duration should be no shorter than the DGD τ. A typical PMD parameter is $D_p = 0.1$ ps/km$^{1/2}$ and therefore, for a fiber length of 5000 km, the mean DGD is $E[\tau] \approx 7$ ps. Assuming the symbol rate per polarization is $R = 26.7$ GHz and assuming 4-QAM-modulated subcarriers, the chip or sample period is about $T_c \approx 35$ ps for 128 subcarriers (Table I). Assuming it is necessary to compensate a DGD of five times the mean in order to achieve low outage probability, the maximum DGD is $\tau_{max} = 5 \, E[\tau] \approx 35$ ps. A cyclic prefix length of only one sample would be sufficient. In practice, the overall power penalty would be dominated by GVD, as it requires a cyclic prefix length of several samples.

An exact analytical form for the Jones matrices describing higher-order PMD has not yet been developed [15], [16]. However, without loss of generality, the configuration in Fig. 11 could be used to mitigate any order of PMD, provided that the cyclic prefix is chosen to be sufficiently long. If the complete statistics were known for higher-order PMD, (11) could be used to estimate the ISI and ICI from the tails of the impulse response not covered by the cyclic prefix, and therefore a design choice could be done for a desired outage probability. However, we believe that using a cyclic prefix somewhat longer than five times the mean DGD should be sufficient to combat almost the entire duration of the impulse response of higher-order PMD [15]. For higher-order PMD, the rotation matrices would need to be frequency-dependent, $\mathbf{R_1}(\omega)$ and $\mathbf{R_2}(\omega)$, while the diagonal matrix $\mathbf{\Lambda}$ would need to include additional powers of ω [15].

B. Single-Polarization Receiver

A single-polarization receiver was already shown in Fig. 1. We assume that polarization control is used such that the LO polarization is locked to the polarization at the carrier frequency. Since only one polarization is detected, the frequency response corresponds to one of the rows of the Jones matrix given by (13). It can be written as

$$H_{PMD}(\omega) = ae^{j\omega\tau/2} + be^{-j\omega\tau/2} \tag{18}$$

where a and b are complex-value constants from the matrices $\mathbf{R_1}$ and $\mathbf{R_2}$. As one can observe, (18) is very similar to multi-path propagation in wireless system. The probability of symbol error for 4-QAM-modulated subcarriers can be written as shown in (19) at the bottom of the page, where $N_u/(N_u + N_{pre})$ is the extra energy wasted on the cyclic prefix samples, P_q is the average power per symbol of each subcarrier, σ_0^2 is the AWGN variance and $H_{PMD}(\omega)$ is the frequency response given by (18). We note again that the cyclic prefix length should be equal to the DGD to avoid ISI as can be seen from the impulse response corresponding to (18), i.e.,

$$P_s = \frac{1}{N_u}\sum_{q=0}^{N_u-1} erfc\left(\sqrt{\frac{1}{2}\left(\frac{N_u}{N_{pre}+N_u}\right)\left(\frac{P_q}{\sigma_0^2}\right)\left(\frac{1}{|H_{PMD}(2\pi q f_c/N_c)|^2}\right)}\right) \tag{19}$$
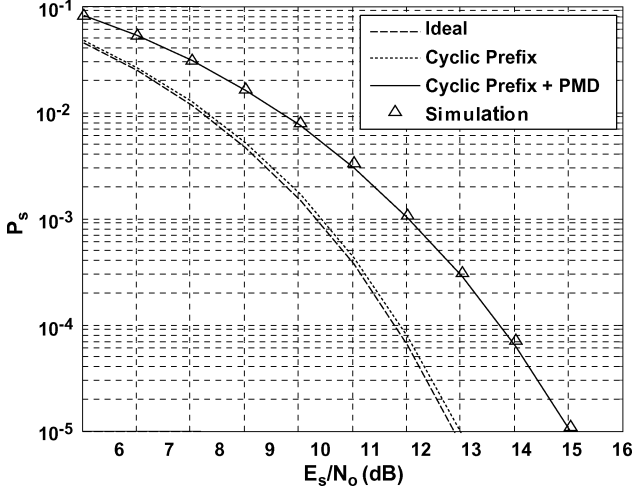
Fig. 12. Probability of symbol error in presence of first-order PMD using a single-polarization receiver, assuming $\tau = 21$ ps, $a| = |b| = 0.5$, $N_u = 52$, $N_c = 64$, $N_{\mathrm{pre}} = 1$ and $R = 26.7$ GHz.

$h_{PMD}(t) = a\delta(t+\tau/2)+b\delta(t-\tau/2)$. However, we point out that while the cyclic prefix can be made long enough to avoid ISI up to a desired outage probability, there is SNR degradation in the single-polarization receiver due to the frequency-dependent attenuation of the channel.

Fig. 12 shows the probability of symbol error for transmission at a symbol rate $R = 26.7$ GHz using 4-QAM-modulated subcarriers. The DGD is $\tau = 21$ ps, i.e., 3 times the mean of a link with 5000 km with $D_p = 0.1$ ps/km$^{1/2}$. As a worst case, equal power splitting between the PSPs ($|a| = |b| = 0.5$) is assumed. The error probability computed using (19) is in good agreement with the simulation results.

V. CONCLUSION

OFDM with a one-tap equalizer is able to compensate for linear distortions such as GVD and PMD, provided that an adequate cyclic prefix length is chosen. Compensation of PMD requires a dual-polarization receiver. We have derived analytical penalties for the ISI and ICI occurring when an insufficient cyclic prefix is used. Using these penalties, we have computed the minimum number of subcarriers and cyclic prefix length required to achieve a specified power penalty for GVD and first-order PMD. We observed that GVD is the dominant impairment, since it requires several cyclic prefix samples, whereas first-order PMD typically requires only one cyclic prefix sample. We verified that an oversampling ratio of 1.2 is sufficient to minimize aliasing. By contrast, single-carrier systems typically require an oversampling ratio of 1.5 or 2 to avoid aliasing.

APPENDIX A

Derivation of the ISI and ICI variance on the different subcarriers is crucial for determining the probability of symbol error. A similar derivation for unilateral channels can be found in [17]. Here, we generalize to bilateral channels and include the effect of correlation when oversampling is used.

If $N_{\mathrm{pre}} = N_{\mathrm{pos}}+N_{\mathrm{neg}}$ samples are used for the cyclic prefix, and if the channel impulse response has positive and negative

lengths $L_p - 1$ and $L_n - 1$, respectively, the residual ISI on the nth time-domain sample in the kth OFDM symbol can be written as

$$
\mathrm{ISI}_k(n) = \sum_{r=N_{\mathrm{pos}}+1}^{L_p-1} x_{k-1}(n+N_c+N_{\mathrm{pre}}+N_{\mathrm{pos}}-r)h_{\mathrm{channel}}(r)
$$
$$
+ \sum_{u=-L_n+1}^{-N_{\mathrm{neg}}-1} x_{k+1}(n-N_c-N_{\mathrm{neg}}-u)h_{\mathrm{channel}}(u) \quad \text{(A1)}
$$

where n varies from 0 to $N_c - 1$. Equation (A1) represents the ISI as a linear function of the OFDM chips. As the number of subcarriers increases, by the Central Limit Theorem [1], the pdf of the chip samples approaches a Gaussian. Since the ISI is a linear function of the chips, its pdf is also Gaussian. The signal after the DFT becomes

$$
\mathrm{ISI}_k(q)
$$
$$
= \sum_{n=0}^{N_c-1} \Bigg(\sum_{r=N_{\mathrm{pos}}+1}^{L_p-1} x_{k-1}(n+N_c+N_{\mathrm{pre}}+N_{\mathrm{pos}}-r)
$$
$$
\times h_{\mathrm{channel}}(r)
$$
$$
+ \sum_{u=-L_n+1}^{-N_{\mathrm{neg}}-1} x_{k+1}(n-N_c-N_{\mathrm{neg}}-u)
$$
$$
\times h_{\mathrm{channel}}(u) \Bigg) e^{-j\frac{2\pi nq}{N_c}}. \quad \text{(A2)}
$$

Performing a variable change on the different sums, we get

$$
\mathrm{ISI}_k(q) = \sum_{n=0}^{N_c-1} \sum_{v=N_{\mathrm{pos}}+1-n}^{L_p-1-n} x_{k-1}(N_c+N_{\mathrm{pre}}+N_{\mathrm{pos}}-v)
$$
$$
\times h_{\mathrm{channel}}(n+v)e^{-j\frac{2\pi nq}{N_c}}
$$
$$
+ \sum_{n=0}^{N_c-1} \sum_{z=N_c-L_n-n}^{N_c-N_{\mathrm{neg}}-2-n} x_{k+1}(-N_{\mathrm{neg}}-1-z)
$$
$$
\times h_{\mathrm{channel}}(n+z-N_c+1)e^{-j\frac{2\pi nq}{N_c}}. \quad \text{(A3)}
$$

Next we interchange the inner and outer sums. In both of the double summations, we require that $N_c > \max(L_p - N_{\mathrm{pos}} - 1, L_n - N_{\mathrm{neg}} - 1)$. This means that the OFDM block must be longer than the impulse response duration or interference from symbols $k+2$ or $k-2$ will take place. In the first double sum, as n increases, the upper limit of the inner sum v decreases accordingly. The lower limit $N_{\mathrm{pos}} + 1$ is reached when $n = L_p - N_{\mathrm{pos}} - 1$. If we now take the sum over v for the outer sum of the first double sum, we obtain the upper limit for the inner sum n as $L_p - 1 - v$. The same idea can be applied to the second double sum, and the lower limit of the inner sum z is reached when $n = L_n - N_{\mathrm{neg}} - 1$. If we now take the sum over z for the outer sum of the second double sum, we obtain the lower limit for the inner sum n as $N_c - L_n - z$. Thus, (A3) becomes

$$
\mathrm{ISI}_k(q) = \sum_{v=N_{\mathrm{pos}}+1}^{L_p-1} \sum_{n=0}^{L_p-1-v} h_{\mathrm{channel}}(n+v)x_{k-1}
$$
$$
\times (N_c+N_{\mathrm{pre}}+N_{\mathrm{pos}}-v)e^{-j\frac{2\pi nq}{N_c}}
$$

$$+ \sum_{z=-L_n+1}^{-N_{\text{neg}}-1} \sum_{n=N_c-L_n-z}^{N_c-1} h_{\text{channel}}(n+z-N_c+1)$$
$$\times x_{k+1}(-N_{\text{neg}}-1-z)e^{-j\frac{2\pi nq}{N_c}}. \quad (A4)$$

Substituting $n+v=p$ and $n+z=m$ in the first and second double sums, respectively, we get

$$\text{ISI}_k(q) = \sum_{v=N_{\text{pos}}+1}^{L_p-1} x_{k-1}(N_c+N_{\text{pre}}+N_{\text{pos}}-v)$$
$$\times \sum_{p=v}^{L_p-1} h_{\text{channel}}(p)e^{-j\frac{2\pi(p-v)q}{N_c}}$$
$$+ \sum_{z=-L_n+1}^{-N_{\text{neg}}-1} x_{k+1}(-N_{\text{neg}}-1-z)$$
$$\times \sum_{m=N_c-L_n}^{N_c-1-z} h_{\text{channel}}(m-N_c+1)e^{-j\frac{2\pi(m-z)q}{N_c}}$$
$$= \sum_{v=N_{\text{pos}}+1}^{L_p-1} x_{k-1}(N_c+N_{\text{pre}}+N_{\text{pos}}-v)e^{j\frac{2\pi vq}{N_c}}$$
$$\times \sum_{p=v}^{L_p-1} h_{\text{channel}}(p)e^{-j\frac{2\pi pq}{N_c}}$$
$$+ \sum_{z=-L_n+1}^{-N_{\text{neg}}-1} x_{k+1}(-N_{\text{neg}}-1-z)e^{j\frac{2\pi zq}{N_c}}$$
$$\times \sum_{m=N_c-L_n}^{N_c-1-z} h_{\text{channel}}(m-N_c+1)e^{-j\frac{2\pi mq}{N_c}}$$
$$= \sum_{v=N_{\text{pos}}+1}^{L_p-1} x_{k-1}(N_c+N_{\text{pre}}+N_{\text{pos}}-v)$$
$$\times e^{j\frac{2\pi vq}{N_c}} H_v(q)$$
$$+ \sum_{z=-L_n+1}^{-N_{\text{neg}}-1} x_{k+1}(-N_{\text{neg}}-1-z)$$
$$\times e^{j\frac{2\pi zq}{N_c}} H_z(q). \quad (A5)$$

Note that the expressions for $H_v(q)$ and $H_z(q)$ correspond to the DFTs of the positive and negative tails of the channel impulse response $h_{\text{channel}}(n)$. After the DFT, the variance $\sigma_{\text{ISI}}^2(q)$ on each subcarrier q is

$$\sigma_{\text{ISI}}^2(q) = E[ISI(q)ISI^*(q)]$$
$$= \sum_{v1=N_{\text{pos}}+1}^{L_p-1} \sum_{v2=N_{\text{pos}}+1}^{L_p-1} H_{v1}(q)H_{v2}(q)^*$$
$$\times E[x_{k-1}(N_c+N_{\text{pre}}+N_{\text{pos}}-v_1)$$
$$\times x_{k-1}(N_c+N_{\text{pre}}+N_{\text{pos}}-v_2)^*]$$
$$\times e^{j\frac{2\pi(v_1-v_2)q}{N_c}}$$
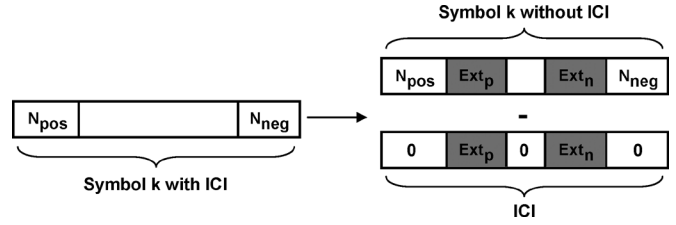$$+ \sum_{z1=-L_n+1}^{-N_{\text{neg}}-1} \sum_{z2=-L_n+1}^{-N_{\text{neg}}-1} H_{z1}(q)H_{z2}(q)^*$$

Fig. 13. OFDM symbol extension for computing the ICI.

$$\times E[x_{k+1}(-N_{\text{neg}}-1-z_1)$$
$$\times x_{k+1}(-N_{\text{neg}}-1-z_2)^*]e^{j\frac{2\pi(z_1-z_2)q}{N_c}}$$
$$+ \sum_{v1=N_{\text{pos}}+1}^{L_p-1} \sum_{z1=-L_n+1}^{-N_{\text{neg}}-1} H_{v1}(q)H_{z1}(q)^*$$
$$\times E[x_{k-1}(N_c+N_{\text{pre}}+N_{\text{pos}}-v_1)$$
$$\times x_{k+1}(-N_{\text{neg}}-1-z_1)^*]e^{j\frac{2\pi(v_1-z_1)q}{N_c}}$$
$$+ \sum_{z2=-L_n+1}^{-N_{\text{neg}}-1} \sum_{v2=N_{\text{pos}}+1}^{L_p-1} H_{z2}(q)H_{v2}(q)^*$$
$$\times E[x_{k+1}(-N_{\text{neg}}-1-z_2)$$
$$\times x_{k-1}(N_c+N_{\text{pre}}+N_{\text{pos}}-v_2)^*]$$
$$\times e^{j\frac{2\pi(z_2-v_2)q}{N_c}}. \quad (A6)$$

If we assume that the symbols are uncorrelated, i.e., $E[x(n)_k x(l)_m^*] = 0$ for $n \neq l$, (A6) simplifies to

$$\sigma_{\text{ISI}}^2(q) = \sigma_s^2 \left(\sum_{v=N_{\text{pos}}+1}^{L_p-1} |H_v(q)|^2 + \sum_{z=-L_n+1}^{-N_{\text{neg}}-1} |H_z(q)|^2 \right) \quad (A7)$$

where $\sigma_s^2 = E[|x(n)|^2]$ is the mean power per sample of the time-domain waveform. Equation (A7) gives the variance of the interference induced on subcarrier q in the OFDM symbol k by the previous and subsequent symbols, $k-1$ and $k+1$. It remains now to calculate the interference caused by the current symbol k on itself, i.e., the ICI. ICI occurs because when the cyclic prefix is not sufficiently long, linear convolution between the channel and symbol k does not correspond to one period of a circular convolution. In order to compute the ICI, we assume an extension within the received symbol k so that it is equivalent to one period of a circular convolution between the channel and the transmitted symbol k. The removal of this extension would then be the ICI. The extension concept is illustrated in Fig. 13.

The ICI is then similar to (A1) and can be written as

$$\text{ICI}_k(n) = - \sum_{r=N_{\text{pos}}+1}^{L_p-1} x_k(n+N_c+N_{\text{pre}}+N_{\text{pos}}-r)h_{\text{channel}}(r)$$
$$- \sum_{u=-L_n+1}^{-N_{\text{neg}}-1} x_k(n-N_c-N_{\text{neg}}-u)h_{\text{channel}}(u). \quad (A8)$$

If we follow the same steps as in derivation of the ISI, we see that the ICI and ISI differ only by a sign, which disappears when squaring to compute the variance. Hence, the ISI and ICI have

the same variance, $\sigma_{\text{ISI}}^2(q) = \sigma_{ICI}^2(q)$. Thus, the variance of the total interference on subcarrier q can be written as

$$\sigma_{\text{ISI+ICI}}^2(q) = 2\sigma_s^2\left(\sum_{v=N_{\text{pos}}+1}^{L_p-1}|H_v(q)|^2 + \sum_{z=-L_n+1}^{-N_{\text{neg}}-1}|H_z(q)|^2\right). \tag{A9}$$

Equations (A7) and (A9) are exact when the OFDM chips are uncorrelated. However, if oversampling is used, the chips are no longer uncorrelated and therefore (A7) and (A9) represent an approximation.

ACKNOWLEDGMENT

REFERENCES

[1] G. L. Stuber, *Principles of Mobile Communication*, 2nd ed. Boston, MA: Kluwer Academic, 2001.

[2] K. Sistanizadeh, P. Chow, and J. M. Cioffi, "Multitone transmission for Asymmetric Digital Subscriber Lines (ADSL)," in *Proc. ICC'91*, Geneva, Switzerland, May 23–26, 1993, pp. 756–760.

[3] W. Shieh, "PMD-supported coherent optical OFDM systems," *IEEE Photon. Technol. Lett.*, vol. 19, no. 3, pp. 134–136, Feb. 2007.

[4] S. L. Jansen, I. Morita, N. Takeda, and H. Tanaka, "20-Gb/s OFDM transmission over 4160 km SSMF enabled by RF-pilot tone phase noise compensation," in *OFC 2007*, Anaheim, CA, postdeadline paper PDP15.

[5] B. Schmidt, A. Lowery, and J. Armstrong, "Experimental demonstration of 20 Gb/s direct-detection optical OFDM and 12 Gb/s with a colorless transmitter," in *OFC 2007*, Anaheim, CA, postdeadline paper PDP18.

[6] Y. Tang, W. Shieh, X. Yi, and R. Evans, "Optimum design for RF-to-optical up-converter in coherent optical OFDM systems," *IEEE Photon. Technol. Lett.*, vol. 19, no. 7, pp. 483–485, Apr. 2007.

[7] A. Lowery, S. Wang, and M. Premaratne, "Calculation of power limit due to fiber nonlinearity in optical OFDM systems," *Opt. Expr.*, vol. 15, no. 20, pp. 13282–13287, Sep. 2007.

[8] S. Wu and Y. Bar-Ness, "OFDM systems in the presence of phase noise: Consequences and solutions," *IEEE Trans. Commun.*, vol. 52, no. 11, pp. 1988–1996, Nov. 2004.

[9] K. Ho and J. M. Kahn, "Spectrum of externally modulated optical signals," *J. Lightw. Technol.*, vol. 22, no. 2, pp. 658–663, Feb. 2004.

[10] E. Ip and J. M. Kahn, "Digital equalization of chromatic dispersion and polarization mode dispersion," *J. Lightw. Technol.*, vol. 25, no. 8, pp. 2033–2043, Aug. 2007.

[11] T. M. Schmidl and D. C. Cox, "Robust frequency and timing synchronization for OFDM," *Trans. Commun.*, vol. 45, no. 12, pp. 1613–1621, Dec. 1997.

[12] J.-J. van de Beek, M. Sandell, and P. O. Borjesson, "ML estimation of time and frequency offset in OFDM systems," *Trans. Signal Process.*, vol. 45, no. 12, pp. 1800–1805, Jul. 1997.

[13] G. J. Foschini and C. D. Poole, "Statistical theory of polarization dispersion in single mode fibers," *J. Lightw. Technol.*, vol. 9, pp. 1439–1456, Nov. 1991.

[14] E. Forestieri and G. Prati, "Exact analytical evaluation of second-order PMD impact on the outage probability for a compensated system," *J. Lightw. Technol.*, vol. 22, no. 4, pp. 988–996, Apr. 2004.

[15] E. Forestieri and L. Vincetti, "Exact evaluation of the Jones matrix of a fiber in the presence of polarization mode dispersion of any order," *J. Lightw. Technol.*, vol. 19, no. 12, pp. 1898–1909, Dec. 2001.

[16] H. Kogelnik, L. E. Nelson, J. P. Gordon, and R. M. Jopson, "Jones matrix for second-order polarization mode dispersion," *Opt. Lett.*, vol. 25, no. 1, pp. 19–21, Jan. 2000.

[17] W. Henkel, G. Taubock, P. Odling, P. O. Borjesson, and N. Petersson, "The cyclic prefix of OFDM/DMT—An analysis," presented at the IEEE Seminar on Broadband Communications, Zurich, Switzerland, 2002.

Daniel J. F. Barros received the *Licenciatura* degree (with honors) in electrical and electronics engineering from the University of Porto, Portugal, in 2004, and the M.S. degree in electrical engineering from Stanford University, Stanford, CA, in 2007, where he is currently working towards the Ph.D. degree in electrical engineering.

His research interests include single-mode optical-fiber communication, digital signal processing and RF circuits.

Joseph M. Kahn (M'90–SM'98–F'00) received the A.B., M.A., and Ph.D. degrees in physics from the University of California, Berkeley, in 1981, 1983, and 1986, respectively.

From 1987 to 1990, he was with AT&T Bell Laboratories, Crawford Hill Laboratory, Holmdel, NJ. He demonstrated multigigabits-per-second coherent optical-fiber transmission systems, setting world records for receiver sensitivity. From 1990 to 2003, he was a faculty member with the Department of Electrical Engineering and Computer Sciences, University of California, Berkeley, performing research on optical and wireless communications. In 2000, he helped found StrataLight Communications, where he served as Chief Scientist from 2000 to 2003. Since 2003, he has been a Professor of electrical engineering with Stanford University, Stanford, CA. His current research interests include single and multimode optical-fiber communications, free-space optical communications, and microelectromechanical systems for optical communications.

Prof. Kahn was the recipient of the National Science Foundation Presidential Young Investigator Award in 1991. From 1993 to 2000, he served as a Technical Editor of *IEEE Personal Communications Magazine*.